The First Metal-Rich Binary Chalcogenides of the Lanthanides: Dy_2Te and Gd_2Te

P. Subramanya Herle and John D. Corbett*

Department of Chemistry, Iowa State University, Ames, Iowa 50011

Received November 16, 2000

Two new tellurides have been synthesized in Ta with particular attention to the use of finely divided Dy (Gd) and a sequence of reactive sintering reactions of pressed pellets up to ~1060 °C. Both phases disproportionate to Ln and LnTe at only slightly higher temperatures so that arc-melting procedures are relatively unproductive. The two compounds crystallize with a Sc_2Te-type structure. Single-crystal X-ray diffraction results for Dy_2Te were detailed in the orthorhombic space group *Pnma* (No. 62), $Z = 12$, $a = 21.922(4)$ Å, $b = 4.0650(6)$ Å, and $c = 11.428(2)$ Å (Guinier data). There is good evidence for the existence of additional metal-rich binary chalcogenides of the heavy lanthanides. Extended Hückel calculations were performed within the tight binding approximation to aid the understanding of the metal−metal bonding in this system. In terms of metal−metal overlap populations, the isotypic Sc_2Te is more 1D in aggregation, while the larger atoms and orbitals and stronger bonding in Dy_2Te make it somewhat more 3D. Electrical resistivity and magnetic susceptibility measurements on polycrystalline Dy_2Te indicate it is metallic and ferromagnetic (T_c= 161.3 K) with an effective moment at higher temperatures close to that of ground-state Dy^{3+}. The connections between heavy lanthanide-rich chalcogenide chemistry and that of the early transition metals seem significant.

Introduction

The many metal-rich binary chalcogenides discovered for the earlier transition metals have greatly expanded our understanding of their chemistry, structures, and metal−metal bonding. The collection exhibits a remarkable range of compositions and structures, even among the M_2Ch examples (M = Sc, Ti, Zr, Hf, Nb, Ta; Ch = S, Se, Te) with their diverse range of often novel structures.[1−12] This is part of a rapidly growing area of solid-state chemistry wherein the normal building blocks in new structure types are low-dimensional metal chains and sheets separated by chalcogenide anions. The first binary example of the rare-earth metals, Sc_2Te, provided a new structure type with chains of condensed metal clusters running parallel to the short repeat axis.[1] The electron-richer β-Ti_2Se[9] and Zr_2Te[11] have recently been shown to exhibit Sc_2Te-type structures as well, with increased bonding being evident. Other examples of reduced binary chalcogenides of the earlier transition metals include, but are not limited to, R_8Te_3 (R = Sc, Y)[13] and Sc_9Te_2,[14] Ti_8Ch_3 (Ch = S, Se),[15,16] $Ti_{11}Se_4$,[17] Ti_9Se_2,[18] and Zr_3Te.[19] Many of these compounds have the common feature of a short crystallographic axis that is about the van der Waals diameter of the chalcogenide anion (~3.6−4.0 Å).

In preparative solid-state chemistry, it is not possible to predict either whether some hypothetical compound will exist or what structure it will exhibit. Successful preparative routes to metal-rich lanthanide chalcogenides have previously been unavailable, and we can only guess why. Several groups have reported how new binary metal-rich phases of neighboring transition metals may be synthesized by high-temperature techniques, and these are often very effective when both the metals and the compounds sought are refractory. A long-used route has been to start with some prereaction to bind the chalcogen and then to arc-melt the components and anneal that product at lower temperatures.[19] However, evidently all successful syntheses of binary lanthanide chalcogenides to date have utilized glass or fused silica containers, for which their reactivity with the active metal and perhaps the products at the necessary temperatures has limited the useful products to LnCh, Ln_3Ch_4, and higher analogues. For example, syntheses of the fairly common LnCh (NaCl type) compounds has generally utilized a prior reaction of the 1:1 elements in glass up to 400−450 °C, after which the intermediate metal−chalcogenide mixture was pressed into a pellet, sealed into an evacuated fused silica container, and slowly heated to 1000−1100 °C. The products were stated to be 99+% pure.[20] It seems rather clear that much better inertness, higher useful temperatures, and metal-richer products should be achievable with tantalum containers, the use of which is now fairly

(1) Sc_2Te: Maggard, P. A.; Corbett, J. D. *Angew. Chem., Int. Ed. Engl.* **1997**, *36*, 1974.
(2) Ti_2S: Owens, J. P.; Franzen, H. F. *Acta Crystallogr.* **1967**, *23*, 77.
(3) Zr_2S: Conard, B. R. *High Temp. Sci.* **1971**, *3*, 491.
(4) Hf_2S: Franzen, H. F. *Z. Kristallogr.* **1966**, *123*, 1331.
(5) Ta_2S: Franzen, H. F.; Smeggil, J. G. *Acta Crystallogr.* **1969**, *B25*, 1736.
(6) Zr_2Se: Franzen, H. F. *Acta Crystallogr.* **1968**, *B24*, 801.
(7) Ti_2Se, Hf_2Se: Franzen, H. F.; Smeggil, J.; Conard, B. R. *Mater. Res. Bull.* **1967**, *2*, 1087.
(8) Ti_2Se: Weirich, T. E.; Pöttgen, R.; Simon, A. *Z. Kristallogr.* **1996**, *211*, 928.
(9) β-Ti_2Se: Weirich, T. E.; Zou, X.; Ramlau, R.; Simon, A.; Cascarano, G. L.; Giacovazzo, C.; Hovmoller, S. *Acta Crystallogr.* **2000**, *A56*, 29.
(10) Ta_2Se: Harbrecht, B. *Angew. Chem., Int. Ed. Engl.* **1989**, *28*, 1660.
(11) Zr_2Te: Örlygsson, G.; Harbrecht, B. *Inorg. Chem.* **1999**, *38*, 3377.
(12) Hf_2Te: Harbrecht, B.; Conrad, M.; Degen, T.; Herbertz, R. *J. Alloys Compd.* **1997**, *255*, 178.
(13) Maggard, P. M.; Corbett, J. D. *Inorg. Chem.* **1998**, *37*, 814.
(14) Maggard, P. M.; Corbett, J. D. *J. Am. Chem. Soc.* **2000**, *122*, 838.
(15) Owens, J. P.; Franzen, H. F. *Acta Crystallogr.* **1974**, *B30*, 427.
(16) Weirich, T. E.; Pöttgen, R.; Simon, A. *Z. Kristallogr.* **1996**, *211*, 929.
(17) (a)Weirich, T. E.; Ramlau, R.; Simon, A.; Hovmöller, S.; Zou, X. *Nature* **1996**, *382*, 144. (b) Weirich, T. E.; Simon, A.; Pöttgen, R. *Z. Anorg. Allg. Chem.* **1996**, *622*, 630.
(18) Harbrecht, B.; Leersch, R *J. Alloys Compd.* **1996**, *238*, 13.
(19) Franzen, H. F. *J. Solid State Chem.* **1986**, *64*, 283.
(20) Wetzel, K. In *Handbook of Preparative Inorganic Chemistry*, 2nd ed.; Brauer, G., Ed., Academic Press: New York, Vol. 2, 1965; p 1155.

10.1021/ic0012975 CCC: $20.00 © 2001 American Chemical Society
Published on Web 03/14/2001

routine.[21] The metal-rich Ln−Ch systems are naturally important not only because of their unknown compositions, structures, and bonding but also because the localized 4f core electrons contribute to novel magnetic and electrical properties. Here we report on our exploratory syntheses in the Dy−Te, Gd−Te, and some related systems. We have already reported on the new ternary dysprosium telluride phases Dy_6MTe_2 for M = Fe, Co, Ni, Pt, for which the necessary synthetic conditions seem to be less limiting.[22] Note also that we distinguish herein between the *lanthanide* elements with their greater similarities of properties and the *rare-earth* metals which also include Sc and Y.

Experimental Section

Syntheses. All materials were handled in a He-filled glovebox. Preliminary studies on the synthesis of Dy-rich chalcogenides utilized prereactions of Dy pieces (Ames Lab, 99.9% total) with Te (Alfa-Aesar, 99.998%) at the desired overall composition in sealed, evacuated SiO_2 jackets at 600 °C for ~2 days. The products appeared to be free of contaminants, but 6 days at 600 °C instead, or 3 days at 700 °C, produced a Dy_2O_2Te impurity according to Guinier powder diffraction. The intent of this initial stage was to reduce the Te activity sufficiently to avoid its subsequent loss by either volatilization or its sometimes vigorous reaction with Ta. Such a prereacted sample, which usually contained Dy, Dy_2Te_3, and Dy_2Te_5, was then ground, pelletized, and arc-melted. However, this produced only a mixture of shiny submillimeter Dy spheres, partially aggregated, in a matrix of red-brown DyTe. The last is the highest melting product (~1850 °C) in the current 1970 version of the binary Dy−Te phase diagram.[23] (This diagram is devoid of any Dy-richer phases, probably because glassy carbon containers were used during synthesis reactions in that region.[24]) Although subsequent annealing of these samples sealed within 9-mm in. i.d. Ta containers (further jacketed in a sealed fused silica tube) at 1000−1100 °C for a few days gave evidence for some new phases, the X-ray diffraction intensities of these were generally weak and diffuse, and the reactions, too incomplete.

Thereafter, reactions of powdered metal with Te and the avoidance of any arc-melting steps were found to afford much better routes to Dy-rich compounds. The metal powder was prepared by filing Dy rod in the glovebox, and this in a 2:1 (or other) proportion with Te was heated at 600 °C within an evacuated (~10^{-6} Torr) sealed SiO_2 tube for 48 h. The product then consisted mainly of poorly crystalline Dy, Dy_2Te, and DyTe. (A powder prepared by thermal decomposition of $DyH_{\sim 2}$ in a vacuum appeared to work as well.) This prereacted sample was then ground, pressed into a 5 mm diameter pellet (~6 tons per cm^2) within a glovebox, and then sealed in Ta under Ar, the container of choice for all subsequent reactions. Equilibration at 950 °C for 2 days (following heating from 600 °C at 0.2 °C min/h) yielded new phases mixed with DyTe and Dy according to Guinier film data. (On the other hand, powder patterns of samples following higher rates of heating between 600 and 950 °C appeared to contain higher proportions of DyTe.) After regrinding, a second pressed pellet annealed at 1060 °C for 2 days (after heating from 950 °C at 0.5 °C/min) yielded Guinier film data for single phase (>95%) orthorhombic Dy_2Te, isostructural with Sc_2Te.[1] Suitable single crystals were obtained after a pair of grind−pelletize−anneal sequences at 1060 °C for 5 days and were slowly cooled to room temperature. The Dy_2Te decomposes incongruently above about 1070 °C into DyTe and Dy metal. While the initial synthesis conditions for Gd_2Te were the same as Dy_2Te, the final annealing temperature had to be no higher than ~1050 °C, because the sample likewise disproportionated into GdTe and Gd metal much above this temperature. Exploratory investigations of reactions of other lanthanide elements with Te utilized the same quality materials and methods.

Table 1. Lattice Dimensions (Å, Å^3) of Dy_2Te, Gd_2Te, and Other Compounds with a Sc_2Te-Type Structure (*Pnma*)

compound	*a*	*b*	*c*	*V*
Sc_2Te[a,b]	20.178(5)	3.9186(7)	10.675(2)	844.1(5)
Dy_2Te[a]	21.922(4)	4.0650(6)	11.428(2)	1018.43(2)
Gd_2Te[a]	22.492(6)	4.050(1)	12.064(3)	1099.05(3)
β-Ti_2Se[c]	17.93(2)	3.453(1)	9.526(10)	590(2)
Zr_2Te[d]	19.950(2)	3.8236(2)	10.6563(9)	812.9(2)

[a] Guinier data, 23 °C, λ = 1.74056 Å. [b] Ref 1. [c] Ref 9. [d] Ref 11.

Table 2. Some Crystal and Structure Refinement Data for Dy_2Te

fw	452.60
space group, *Z*	*Pnma* (No. 62), 12
d_{calc}, g/cm^3	8.897
abs coeff, mm^{-1}	52.04
residuals: *R*; R_w[b]	0.035; 0.035

[a] Cell dimensions from Guinier data are given in Table 1. [b] $R = \sum||F_o| - |F_c||/\sum|F_o|$; $R_w = [\sum w(|F_o| - |F_c|)^2/\sum w(F_o)^2]^{1/2}$; $w = \sigma_F^{-2}$.

Powder Diffraction. Diffraction patterns of the powdered products were obtained with the aid of an Enraf-Nonius Guinier camera and monochromatized Cu Kα radiation. The brittle samples were crushed into fine powder, mixed with standard silicon (NIST), and placed on a frame between two strips of cellophane tape for mounting in the camera. The orthorhombic lattice parameters for Dy_2Te and Gd_2Te listed in Table 1 were obtained by least-squares refinements of the indexed and measured 2θ values relative to the Si standard, as before.[13,14] These more accurate lattice dimensions were used in the later calculations of distances from refined single-crystal parameters for Dy_2Te.

EDS Analysis. The composition of a Dy_2Te sample was checked with the aid of a JEOL 840A scanning electron microscope (SEM) equipped with IXRF Systems iridium X-ray analyzer. DyTe was used as an external standard. A few potential single crystals of irregular morphology were chosen for composition analysis. These were found to be $Dy_{66.48(1)}Te_{33.49(4)}$ in atom %, or $Dy_{1.985(2)}Te$ in proportion, very close to the crystallographic composition Dy_2Te. No impurity elements were detected.

Single-Crystal Structural Studies. Several silvery crystals with irregular shapes were mounted in 0.2 mm i.d. thin-walled capillaries that were afterward sealed off and mounted on metal pins. Crystal qualities were checked with Laue photographs, and the best (but small) crystal was chosen for the data collection on a Rigaku AFC6R diffractometer with the aid of graphite-monochromatized Mo Kα radiation. Provisional unit cell dimensions were obtained from least-squares refinement of 12 centered reflections. One-half sphere of data ($\pm h$, $\pm k$, l) was collected and subsequently corrected for polarization effects. An empirical absorption correction was applied with the aid of a ψ scan, which resulted in relative transmission factors ranging from 0.34 to 1.0. (Only one suitable reflection could be found near χ ~90°.) Of 6207 reflections collected ($2\theta \leq 60°$), 1799 were unique (R_{int} = 0.346, R_{av} = 0.133 for $I/\sigma_I > 1$). The absence conditions (0kl: $k + l = 2n$; hk0: $h = 2n$) suggested space groups *Pnma* (No. 62) and $Pna2_1$ (No. 33). The intensity statistics indicated a centrosymmetric space group, so the structure was solved by direct methods[25] and refined with the package TEXSAN[26] in space group *Pnma*. After isotropic refinement, the data were better corrected for absorption by means of DIFABS.[27] The final refinement converged at $R(F)/R_w$ = 0.035/0.035 for the composition Dy_2Te. Selected crystallographic data, atomic positions, and isotropic-equivalent displacement parameters are given in Tables 2 and 3. Additional data collection and refinement parameters and a complete distance list are in the Supporting Information. These as well as F_o/F_c listings are also available from J.D.C.

(21) Corbett, J. D. *Inorg. Synth.* **1983**, *22*, 15.
(22) Bestaoui, N.; Herle, P. S.; Corbett, J. D. *J. Solid State Chem.* **2000**, *155*, 9.
(23) Massalski, T. B., Okamoto, H., Subramanian, P. R., Kacprzak, L., Eds. *Binary Alloy Phase Diagram*s, 2nd ed.; ASM International: 1990; p 1565.
(24) Abrikosov, N. Kr.; Zinchenko, K. A.; Eliseev, A. A. *Inorg. Mater.* **1970**, *6*, 720.
(25) Sheldrick, M. *SHELXS-86*; Universität Göttingen: Germany 1986.
(26) *TEXSAN for Windows*: Crystal Structure Analysis Package; Molecular Structure Corporation, 1997.
(27) Walker, N.; Stuart, D. *Acta Crystallogr.* **1983**, *A39*, 158.

Table 3. Atomic Coordinates and Isotropic-Equivalent Displacement Parameters for Dy_2Te[a]

atom	*x*	*z*	B_{eq}[b]
Dy1	0.3912(1)	0.1528(3)	0.98(6)
Dy2	0.3402(1)	0.4558(3)	0.93(6)
Dy3	0.2333(1)	0.7349(3)	0.89(6)
Dy4	0.0342(1)	0.1163(3)	0.90(6)
Dy5	0.1470(1)	0.4152(3)	1.08(6)
Dy6	0.9841(1)	0.6125(3)	1.41(6)
Te1	0.0693(2)	0.8509(4)	1.00(8)
Te2	0.3728(2)	0.7135(4)	0.84(8)
Te3	0.2604(2)	0.0199(4)	0.80(8)

[a] $y = 1/4$ for all atoms. [b] $B_{eq} = (8\pi^2/3)\sum_i\sum_j U_{ij} a_i^* a_j^* \vec{a}_i \vec{a}_j$.

Properties. About 30 mg of finely powdered Dy_2Te was sandwiched between two silica rods inside a tightly fitting 3 mm i.d. fused silica tube and sealed under He. Magnetization, magnetic susceptibility, and resistivity data were obtained with the aid of a Quantum Design MPMS SQUID magnetometer and accessories over the temperature range $6 \le T \le 300$ K, the former at a field strength of 1000 Oe. The susceptibility data were corrected for diamagnetism of both the sample holder and the atom cores. Electrical properties of Dy_2Te were measured under vacuum from room temperature to 1.7 K by a four-point dc method. This utilized a rectangular block (7.56 mm × 1.125 mm × 1.0 mm) of Dy_2Te that had been cut from a pellet that had been sintered at 1040 °C for 7 days. The leads were afixed with gold paint.

Band Calculations. Extended Hückel band calculations[28] on Dy_2Te were carried out within the tight-binding approximation at 48 k-points spread over the irreducible wedge. The valence-state ionization energies (H_{ii}'s) were values previously obtained for Dy_6FeTe_2 from charge-consistent iterations.[22] These values were, in eV, for Dy 6s, −6.76; 6p, −4.20; 5d, −6.37; Te 5s, −21.2; 5p, −12.0. The exponents ς_1 and ς_2 in the double-ς expansion for the d orbitals and the coefficients c_1 and c_2 of the Slater-type orbitals were taken from Alvarez,[29] as were the ς_1 exponents for Te.

Results and Discussion

Syntheses. The lanthanides appear to form a good number of metal-rich binary chalcogenides, the tellurides in particular that we have principally investigated so far. The coupled problems of a suitably inert container, the attainment of sufficient reaction temperatures in rather refractory systems, and the relatively low decomposition temperatures of the new products are probable reasons why these have not been reported before. The yields were much better when starting with a powdered Dy made by filing. On the other hand, the product of any subsequent arc-melting of the prereacted Dy, Gd mixtures contained no evidence of new phases, rather only a mixture of shiny Dy metal spheres in a dark red-brown matrix of DyTe, presumably because of the relatively low temperature at which Dy_2Te disproportionates, ∼1070 °C. Annealing this product at 1000 °C for a few days showed evidence of several new phases Dy_xTe, $x > 1$, but the yields were low (<∼30%). Successful syntheses came about instead via the so-called ceramic method in which at least two grind−pelletize−anneal sequences were followed by reactions for up to 2−15 days at no higher than 1060 °C for Dy_2Te and 1050 °C for Gd_2Te. On the other hand, this more restrictive synthetic approach is not necessary for the ternary Dy_6MTe_2 phases, M = Fe, Co, Ni,[22] where arc-melting of Dy, M, and $DyTe_2$ directly followed by annealing gave high yields (∼95%, + DyTe). Presumably, the high-temperature phase relationships with the 3d metal lead to much less severe decomposition than for Dy_2Te, etc.

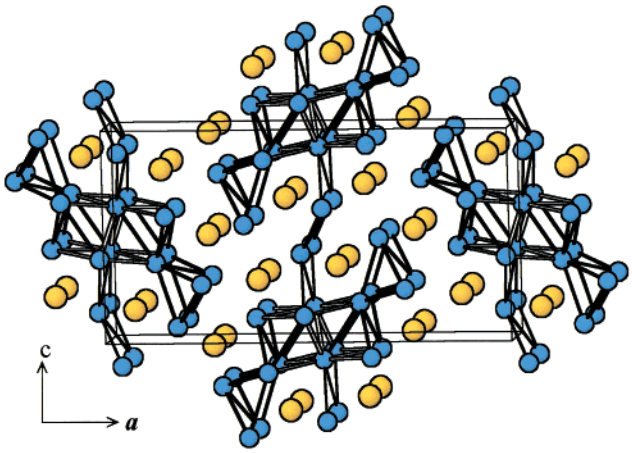

Figure 1. Section of the unit cell of Dy_2Te viewed near [010] with Dy as blue and Te as golden ellipsoids. Dy−Dy bond widths are weighted according to Mulliken overlap populations for those > 0.1.

It is already clear that these methods can also be used to obtain more reduced chalcogenides, especially for the heavier lanthanides.[30] Mixtures containing Ln_8Te_3 phases that appear isostructural with Sc_8Te_3[13] have been seen for Ln = Gd, Dy, and the existence of Ln_9Te_2 for the same Ln seems probable, in parallel with Sc_9Te_2[14] but so far in lower yields. These compounds generally have lower decomposition temperatures than Ln_2Te. There is no indication of new phases between DyTe and Dy_2Te. Metal-rich tellurides and selenides of lutetium also exist. On the other hand, metal-rich binary compounds between La or Pr and Te or Se have not been attained in the range 700−1000 °C by these methods. In a related investigation, $Ln_5Ni_2Te_2$ phases for Ln = Gd, Dy, isostructural with $Y_5Ni_2Te_2$,[31] have evidently been obtained in 60−75% yields.[32]

Structural Description. The new Dy_2Te is isostructural with Sc_2Te,[1] but with some appreciable differences in detail that might be expected because of a significant increase in the metal's classical radius as well as orbital size and bond strength. The same is evident in Sc_2Te−Zr_2Te comparisons, but in this case an increase in valence electron count affects other bonding properties as well.

The unit cell projection for Dy_2Te slightly off [010], the short axis (4.06 Å), is shown in Figure 1 with Dy as blue and Te as golden ellipsoids. The structure contains two types of interconnected metal units separated by telluride in mono-, bi-, and tricapped trigonal prisms of metal: zigzag Dy4 chains and centrosymmetric 10-member condensed chains or blades that contain a diversity of Dy−Dy distances, as detailed in a perspective drawing in Figure 2. The more complex metal chain can be described geometrically starting with a pair of single chains of infinite trans-edge-sharing distorted octahedra that have been fused at Dy6−Dy6. Such double chains are individually related to the metal units (without Ru) in the monoclinic metal-rich halide Pr_3I_3Ru,[34] but the present chain has also been augmented by Dy2 and Dy3 features at the extremes. (The pattern in Figure 2 is easier to understand if it is noted that all adjoining metal neighbors in this projection differ in height by $b/2$, ∼2.0 Å.)

(28) Hoffmann, R. J. *J. Chem. Phys.* **1963**, *39*, 1397. Whangbo, M.-H.; Hoffmann, R.; Woodward R. B. *Proc. R. Soc. London* **1979**, *A366*, 23.
(29) Tables of Parameters for Extended Hückel Calculations, Parts 1 and 2, Alvarez, A., Barcelona, Spain, 1987.
(30) Herle, P. S.; Corbett, J. D. Unpublished research, 2000.
(31) Maggard, P. A.; Corbett, J. D. *J. Am. Chem. Soc.* **2000**, *122*, 10740.
(32) Herle, P. S.; Corbett, J. D. To be submitted for publication.
(33) Pauling, L. *The Nature of the Chemical Bond*, 3rd ed.; Cornell University Press: Ithaca, NY, 1960; p 403.
(34) Corbett, J. D. *J. Alloys Compd.* **1995**, *229*, 10.

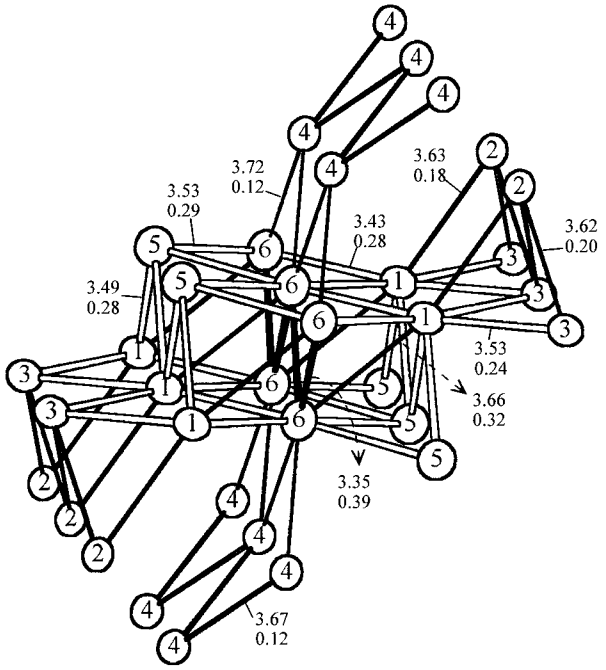

Figure 2. Two-cell section of the metal substructure of Dy_2Te with bond widths weighted as to overlap populations. The numbers indicate the bond distances (Å) and the respective overlap populations.

The shortest distance, Dy6−Dy6 at 3.349 Å, is small compared with the average distance in the hexagonally close-packed metal, 3.56 Å, but it is larger than Pauling's single bond value, 3.20 Å.[33] However, such comparisons are really not very meaningful or useful in such low-symmetry electron-poor aggregates involving highly delocalized metal−metal bonding. The simple, parallel zigzag chains of Dy4 have an internal repeat distance, 3.665 Å, close to the shared octahedral edges Dy1−Dy6 in the large chain, 3.653 Å. However, these interactions in fact represent very different degrees of bonding (below), illustrating the dangers of inferring bond strengths (or relative populations) from distances alone. Thus, the R−R distances listed for Dy_2Te and Sc_2Te in Table 3 are better compared after band calculations and overlap populations are considered.

The more metal-rich chalcogenides with the compositions M_8Ch_3, $M_{11}Ch_4$, and M_9Ch_2 (M = early transition or light rare-earth metal atom, Ch = chalcogen[13−18]) generally contain more condensed metal substructures, often in the form of corrugated sheets composed of condensed octahedra that are separated by chalcogen atoms. From the metal−metal bonding point of view, these are more 2D or 3D in aggregation.

Electronic Structure. Comparisons. The densities-of-states (DOS) diagram for Dy_2Te is shown in Figure 3a. The Fermi level E_F (−7.06 eV) lies in a small local minimum in a broad Dy 5d band, while the Te p orbital contributions occur below −12 eV and, in very small amount, above E_F. The overall width of the conduction band is notably greater than for Sc_2Te and has a closer resemblance to that of Zr_2Te[11] or Ti_2Se.[8] The crystal orbital overlap population (COOP) curves shown in Figure 3b for total Dy−Te and Dy−Dy interactions indicate that the states around and above E_F are bonding and mainly Dy 5d in character, as already noted for the very comparable Sc_2Te. In addition, interactions between the filled states of the Te atoms in such a well-reduced compound are unlikely and, as expected, their pairwise Mulliken overlap populations (OP) are all slightly negative.

The Dy−Dy distances and the pairwise Mulliken overlap populations (OP) are summarized in Table 4 along with the same data for the isoelectronic Sc_2Te. (The latter are otherwise available only in deposited tables. The corresponding Dy−Te

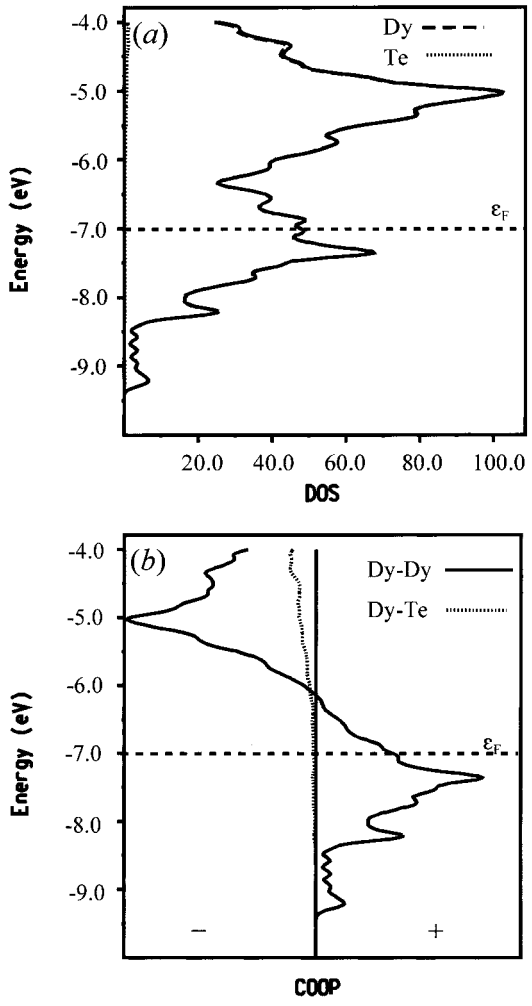

Figure 3. (a) Densities of states (DOS) and (b) crystal orbital overlap populations (COOP) forDy_2Te. The Fermi level is dashed.

Table 4. Selected Interatomic Distances in Dy_2Te and Sc_2Te[a] and the Respective Mulliken Overlap Populations (OP)

	Dy_2Te		Sc_2Te	
atom pair	distance	OP	distance	OP
R6−R6 ×2	3.351(6)	0.394	3.047	0.366
R1−R6 ×2	3.434(3)	0.284	3.126	0.228
R1−R5 ×2	3.493(4)	0.279	3.197	0.172
R1−R3 ×2	3.529(3)	0.239	3.254	0.119
R5−R6	3.533(4)	0.239	3.268	0.146
R2−R3 ×2	3.622(4)	0.198	3.322	0.087
R1−R2	3.629(4)	0.175	3.419	0.069
R1−R6[b]	3.658(1)	0.317	3.486	0.166
R4−R4 ×2	3.668(5)	0.124	3.481	0.026
R4−R6[c] ×2	3.725(4)	0.120	3.530	0.035
R2−R4[c] ×2	3.876(4)	0.074	3.684	0.014
R3−R5[c]	3.905	0.076	3.878	0.009
R2−R3[c]	3.968(4)	0.053	3.726	0.012
R1−R1[d] ×2	4.065(1)	0.110	3.919	0.021
R2−R2[d] ×2	4.065(1)	0.034	3.919	0
R3−R3[d] ×2	4.065(1)	0.134	3.919	0.040
R4−R4[d] ×2	4.065(1)	0.037	3.919	0
R5−R5[d] ×2	4.065(1)	0.045	3.919	0
R6−R6[d] ×2	4.065(1)	0.161	3.919	0.050
R1−R4[c]	4.089(1)	0.062	3.669	0.025
R3−R5[b]	4.107(2)	0.068	3.831	0.007
R5−R6[b]	4.215(1)	0.128	3.519	0.170

[a] Ref 1. [b] Across polyhedra. [c] Interchain distance. [d] Chain repeat along *b*.

information is in the Supporting Information.) The OP data and distances in Dy_2Te are also marked (to one less significant figure) in Figure 2. The discovery of the electron-poor Sc_2Te was important because of the larger degree of physical isolation of the Sc−Sc-bonded metal blade and chain that was brought about by the combination of the small metal with the large anion. Furthermore, bonding orbitals on the metals around the outside of the chains were noted to be raised in energy via polar covalent interactions with their Te neighbors, increasingly so with greater numbers of such neighbors. This effect serves to afford particularly low Sc−Sc overlap populations between nearest metal atoms in the different metal aggregates, through the Te matrix, and also within the isolated zigzag chain, although the Sc−Sc distance in the latter is comparable to some within the larger chain. Distance−overlap population comparisons for Dy_2Te are again remarkable for certain strong interactions within the chain; Dy1−Dy6 in the waist of the imagined octahedra (3.66 Å, OP = 0.317), clearly the region of greatest delocalization, and also, for the distance (3.53 Å) along the height of that octahedron, Dy5−Dy6 (0.239). Also significant contrasts are found for the 4.06 Å chain repeats for Dy6, Dy1, and Dy3 (0.16−0.11). The Dy_2Te-Sc_2Te comparison turns out to be especially fruitful not just because of the ∼0.16 Å larger crystal[35] and metallic[33] radii of dysprosium but particularly because of its substantially larger 5d orbitals and relatively greater Dy−Dy bonding. (Weighing the OP values by the corresponding $-H_{ii}$ for the d orbitals would further enlarge the distinctions between Sc and Dy.[36])

Distance−overlap population (OP) data for Dy_2Te versus Sc_2Te in Table 4 show, first, that in general the R−R distances over the whole bladelike unit marked in Figure 2 have increased in the range 0.21−0.30 Å, less than twice the standard radii difference. However, that in the more or less isolated zigzag Dy4 chain is only 0.14 Å larger, suggesting that anion matrix effects may have been partially responsible for a long 3.48 Å separation along Sc_2Te, as previously surmised. Also, the repeat separation along the chain (*b*), which applies to every atom in the structure, has increased in Dy_2Te but by an even lesser amount, 0.156(1) Å, than within the bladelike unit, suggesting that Dy−Dy orbital interactions are important in this dimension as well, not just the contact diameter of telluride. Within the larger chain, only the proportions of the (condensed) edge-sharing metal octahedra seen in projection have changed substantially, the waist (1−6, marked) and height (5−6) dimensions increasing from those in Sc_2Te (where they were nearly equal) by the contrasting +0.14 and +0.70 Å. Finally, several of the closer interchain separations in Sc_2Te, all of which had very small OP values (<0.035), have increased in Dy_2Te by ≤ 0.19 Å (R3−R5 especially) and have achieved more significant OP values, by up to 0.12, befitting the general expansion of the large chain in a fixed telluride matrix.

The increased d orbital size from Sc 3d to Dy 5d has of course led to generally enhanced overlap in R−R bonds. Mulliken overlap populations are found to have increased accordingly, by 0.09−0.12 per R pair in most parts of the large metal framework, including for the three significant axial repeats (R1,3,6). The exceptions are the two shortest, R6−R6 and R1−R6, which seem to be leveling off in their OP values. As just noted, interchain distances have generally increased less, and so OP values have grown, but these remained fairly small, the largest increase being 0.085 for R4−R6. And the OP within the R4−R4 zigzag chain has increased from 0.03 to 0.20, consistent with the smaller 0.14 Å increase in *d*(R4−R4).

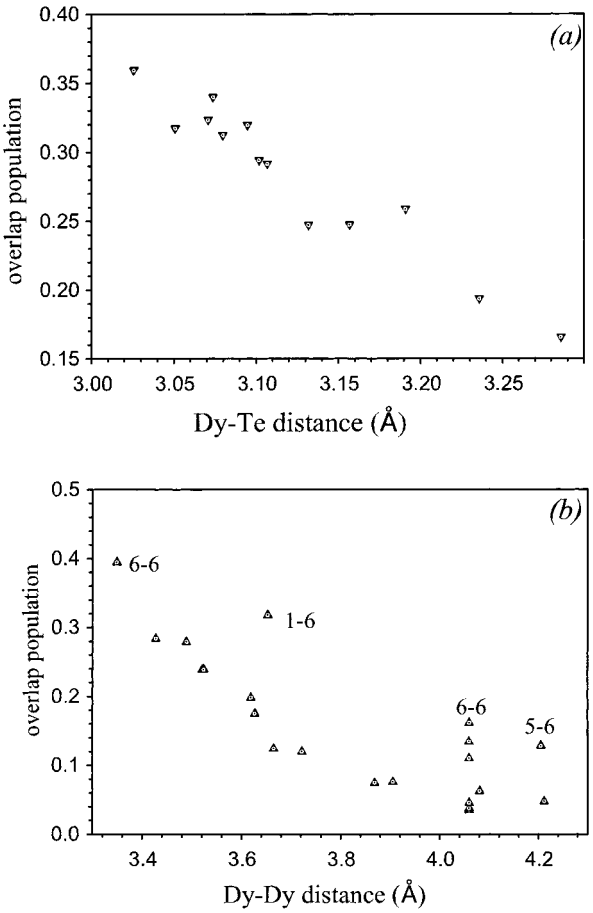

Figure 4. Overlap populations in Dy_2Te as a function of distance for (a) Dy−Te and (b) Dy−Dy atom pairs.

The generally stronger bonding in Dy_2Te can be seen not only in the lower Fermi energy, −7.06 versus −6.4 eV in Sc_2Te, but also from a nearly 60% increase in the width of the filled portion of the large metal d band, which extends only to ca. −7.2 eV in Sc_2Te. Thus, the filled band for the recently described Zr_2Te[11] qualitatively resembles that for Dy_2Te more than does Sc_2Te, presumably because of two opposing effects, the presence of two more valence electrons per formula unit and intermediate strengths (OP) for Zr−Zr bonding. Of course, the chain isolation in the isotypic Ti_2Se[9] is less extreme yet because of the smaller anion, and greater Ti−Ti interactions between the different metal chains lead to more 3D interactions.

The overlap populations for given types of atoms as a function of distance can sometimes be helpful in characterizing different bonding interactions. These are shown in Figure 4 for *d*(Dy−Te) and *d*(Dy−Dy). The OP data for Dy−Te contacts fall off approximately linearly with the distance (see SI), but the data for Dy−Dy pairs scatter around two different curves. Those for interactions between Dy6 and all atoms bonded to it within the condensed Dy chain, namely, Dy6−Dy6 for both the shared edge between chains and the axial repeat and the Dy1−Dy6 and Dy5−Dy6 proportions of the octahedral chains, have significantly higher OP than do other Dy−Dy contacts. Other high values relative to the distance in the upper group pertain especially to the axial repeats for Dy3 and Dy1. Such a clear distinction between OP values for R−R interactions in the interior of the condensed metal structure and lower values for R−R contacts on the exterior that also have Te neighbors was

(35) Shannon, R. D. *Acta Crystallogr.* **1976**, *A32*, 751.
(36) Glassey, W. V.; Hoffmann, R. *J. Chem. Phys.* **2000**, *113*, 1698.

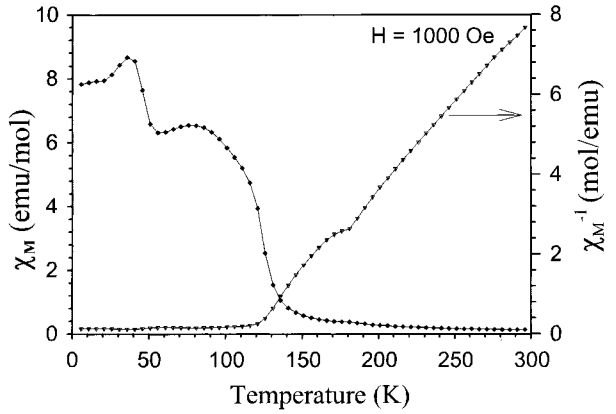

Figure 5. Molar susceptibility and inverse molar susceptibility versus temperature (K) for polycrystalline Dy_2Te at a field strength of 1000 Oe.

first noted in Sc_2Te, but these effects are even clearer here and in Sc_9Te_2.[14]

The second building block in Dy_2Te, the zigzag Dy4−Dy4 chains, does not show any exceptional OP (0.124), but it is clearly better bonded than is Sc4−Sc4 (0.028), both internally and to the other chain at R6, but only in proportion relative to other changes. In general, relatively more secondary bonding between the chains in Dy_2Te makes its bonding somewhat more 3D.

Since the valence electron concentrations remain constant for a series of fixed lanthanide element compositions, one can perhaps attribute overall stability trends to changes in size and bond strengths. Thus radii of the lanthanide elements generally decrease across the series, whereas the cohesive energies of the metals increase. The lower bond strengths and less negative $-H_{ii}$(d) values for La and Pr metals, as reflected in their low melting points (<950 °C), may be the major reasons for our inability to synthesize La_2Te or Pr_2Te or other metal-rich examples. More detailed work is needed to understand the structures and properties of other compounds we have detected.

Magnetic and Electrical Properties. From the metal−metal bonding point of view, significant anisotropy would be expected in the magnetic and electrical properties of Dy_2Te. Of course, hcp Dy metal itself is anisotropic but to a lesser extent. Because our measurements on polycrystalline material show only the average effects, it is difficult to resolve the nature of the magnetic ordering. Figure 5 shows both the molar and the inverse molar susceptibilities of Dy_2Te as a function of temperature at 1000 Oe. The inverse susceptibility can be fitted by a Curie−Weiss expression at the higher temperatures to yield a mean value of $\mu_{eff} = 10.3\ \mu_B$, $\theta = 161.5$ K, whereas the sample becomes ferromagnetic below $T_c = 161.3$ K. Magnetization measurements indicate an increasing hysteresis as the sample is cooled from 110 to 20 K. An antiferromagnetic transition at ∼85 K is reasonable. The nature of the magnetic behavior below 85 K is not clear, but an apparent third transition at ∼50 K is very field dependent. Polycrystalline dysprosium metal shows paramagnetism (10.2−10.4 μ_B) above 179 K, a ferromagnetic transition near 86 K, and antiferromagnetic behavior between 86 and 17.9 K.[37] Although the metal substructure and local environments in Dy_2Te are quite different from those in the metal, its magnetic properties are notably closer to the metal itself than to those of the metallic NaCl-type DyTe.[38]

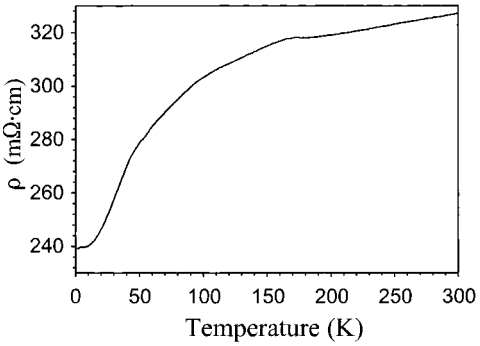

Figure 6. Resistivity data for sintered polycrystalline Dy_2Te.

The zero-field resistivity of polycrystalline sintered Dy_2Te is shown as a function of temperature in Figure 6. The decrease in resistivity from room temperature to 1.7 K indicates a metallic behavior for this material, as expected from the band structure. Although we cannot rule out all effects of impurities such as DyTe and Dy metal (which were undetected and therefore less than ∼3−5% according to the Guinier film analysis), the data should represent the intrinsic behavior of the material. The magnetic transition at ∼170 K is very evident in the slight increase in the resistivity on cooling. Since the measurements were made on a pressed sintered pellet, the data present an average of all orientations and a contribution from grain boundary scattering. Accordingly, the data should represent a higher limit for the resistivities of Dy_2Te. The room-temperature value (330 $\mu\Omega$·cm) is higher than that of Dy metal (91.2 $\mu\Omega$·cm).[39] The resistivities of Dy_2Te fall off quite rapidly between ∼50 and ∼15 K, whereas the sample showed a residual resistivity of ∼240 $\mu\Omega$·cm at 1.7 K, presumably from grain boundaries. Although the same type of resistivity anomaly was observed in single-crystal Dy near 175 K, the values decreased below there somewhat rapidly and linearly.

In contrast, a number of tellurium-rich dysprosium tellurides obey the Curie−Weiss law, without transitions,[40] and the magnetic moments are close to that of Dy^{3+} in its ground state ($^6H_{15/2}$), as are those for Dy metal, Dy_2Te, and DyTe at the higher temperatures. Clearly the 4f electrons in all dysprosium compounds are in localized states. We expect the 5d conduction electrons are responsible for the magnetic ordering in Dy_2Te via a RKKY type interaction.[41] In contrast, Sc metal and its metal-rich tellurides are all appropriately Pauli-paramagnetic.[14] More detailed studies on single-crystal Dy_2Te will be necessary to understand its magnetic properties.

Conclusions

The new lanthanide-rich tellurides Dy_2Te and Gd_2Te have been synthesized by solid-state reaction. The metal-rich portions of the phase diagrams for all lanthanide−chalcogen systems have not been investigated well and systematically in the past, and more detailed studies will definitely uncover more compounds. In general, the lower temperature regions of the phase diagrams of such systems are left open for the synthetic chemist, who must circumvent the decomposition of the desired product during synthesis. The crystal structure of Dy_2Te has been

(37) McEwen, K. A. In *Handbook of the Physics and Chemistry of the Rare Earths*; Gschneidner, K. A., Eyring, L., Eds.; 1978; Vol. 1, Chapter 6.

(38) Pokrzywnicki, S.; Duczmal, M.; Pawlak, L.; Nenkov, K. A. *Acta Phys. Pol., A* **1997**, *92*, 351.

(39) Hall, P. M.; Legovld, S.; Spedding, F. H. *Phys. Rev.* **1960**, *117*, 971.

(40) Pechennikov, A. V.; Kupriyanov, B. A.; Chechernikov, V. I.; Abrikosov, N. Kh.; Zinchenko, K. A. *Izv. Akad. Nauk SSSR, Neorg. Mater*. **1970**, *6*, 1528.

(41) Kittel, C. *Introduction to Solid State Physics*, 7th ed.; John Wiley & Sons: New York, Chichester, 1996; p 628.

determined by single-crystal X-ray diffraction studies to be isostructural with congeneric Sc_2Te. Although Sc_2Te and Dy_2Te adopt the same structure and have the same number of valence electrons, there is a substantial difference in metal−metal bonding in these materials, attributable to the increased cation and valence orbital size and greater bond strength of Dy. The bonding in Dy_2Te (as judged by overlap populations) can be described in terms of condensed distorted octahedral chains and zigzag chains of Dy along *b* that are somewhat better interconnected through the intervening telluride spacers. Magnetic susceptibility measurements on Dy_2Te show a complex behavior, but the Curie−Weiss regime above ~165 K is similar to that in the higher tellurides and dysprosium metal. Electrical resistivity measurements confirmed the metallic behavior. In a bigger picture, the first new results described here and elsewhere[22] for the metal-rich chemistry of the lanthanide chalcogenides make it quite clear that these closely parallel those of the earlier transition metal groups.[1−19] This lanthanide chemistry in the solid state largely involves the higher lying 5d orbitals, so the connection should really not be viewed as particularly surprising or unusual.

Acknowledgment. The synthetic experiments that first signaled the existence of new metal-rich binary dysprosium tellurides were done by N. Bestaoui. The authors thank D.-K. Seo for discussions on theory, Jerome Ostensen for the magnetic measurements, and Ian Fisher and Norman Anderson for the resistivity measurements. This work was supported by the National Science Foundation, Solid State Chemistry, via Grant DMR-9809850, and was carried out in the facilities of the Ames Laboratory, U.S Department of Energy.

Supporting Information Available: Tables of additional crystallographic and refinement parameters, anisotropic thermal parameters, and a complete listing of nearest neighbor distances and Dy−Te overlap populations. This material is available free of charge via the Internet at http://pubs.acs.org

IC0012975